Available online at www.sciencedirect.com
ScienceDirect
Journal of Magnetic Resonance 185 (2007) 230–239
JMR Journal of Magnetic Resonance
www.elsevier.com/locate/jmr

Correlated displacement–T_2 MRI by means of a Pulsed Field Gradient-Multi Spin Echo method

Carel W. Windt, Frank J. Vergeldt, Henk Van As *

Laboratory of Biophysics and Wageningen NMR Centre, Wageningen University, Dreijenlaan 3, 6703 HA Wageningen, The Netherlands

Received 31 October 2006; revised 29 December 2006
Available online 8 January 2007

Abstract

A method for correlated displacement–T_2 imaging is presented. A Pulsed Field Gradient-Multi Spin Echo (PFG-MSE) sequence is used to record T_2 resolved propagators on a voxel-by-voxel basis, making it possible to perform single voxel correlated displacement–T_2 analyses. In spatially heterogeneous media the method thus gives access to sub-voxel information about displacement and T_2 relaxation. The sequence is demonstrated using a number of flow conducting model systems: a tube with flowing water of variable intrinsic T_2's, mixing fluids of different T_2's in an "X"-shaped connector, and an intact living plant. PFG-MSE can be applied to yield information about the relation between flow, pore size and exchange behavior, and can aid volume flow quantification by making it possible to correct for T_2 relaxation during the displacement labeling period Δ in PFG displacement imaging methods. Correlated displacement–T_2 imaging can be of special interest for a number of research subjects, such as the flow of liquids and mixtures of liquids or liquids and solids moving through microscopic conduits of different sizes (e.g., plants, porous media, bioreactors, biomats).

Keywords: Flow; Spin–spin relaxation; Pulsed field gradient; T_2–displacement correlation; Diffusion; Porous media; Plants; Quantification of flow

1. Introduction

Although NMR imaging has been used to image objects as small as a single cell [1,2], the resolution that can be obtained is in general not high enough to resolve structures on a microscopic scale. Inhomogeneous voxels will result when structures in a sample are smaller than can be resolved. To characterize the microscopic internal structure of porous materials and biological tissues, NMR methods are available that are able to overcome this resolution limitation [3–6]. These methods make use of the fact that the NMR properties of the molecules of a fluid inside a porous structure reflect the internal dimensions and geometries. This is valid when the self-diffusion lengths or flow displacements, over timescales comparable with the NMR spin relaxation times, are of a similar order to the structural scales [7,8]. Two main types of NMR experiments are commonly used to investigate porous and biological microstructure: NMR T_2 (spin–spin) and T_1 (spin–lattice) relaxation time measurements, and Pulsed Field Gradient Spin Echo (PFG-SE) or Stimulated Echo (PFG-STE) techniques.

Spin–spin relaxation measurements can provide information on microstructure in microscopically heterogeneous systems, because the relaxation behavior of spins reflects the diffusion of spins to a relaxation-active surface, diffusion within internal magnetic field gradients caused by susceptibility effects, or exchange with relaxation sinks [4,8,9]. In non-imaging mode, T_2 can be measured using a large number of echoes with very short inter echo times and many repetitions. The high signal-to-noise ratio (SNR) of such measurements makes it possible to do a multi-exponential analysis and identify different pools of protons on the basis of relaxation behavior. Spin relaxation measurements combined with imaging methods usually cannot be used in the same manner, because the SNR,

* Corresponding author. Fax: +31 317 482725.
E-mail address: Henk.Vanas@wur.nl (H. Van As).

1090-7807/$ - see front matter © 2007 Elsevier Inc. All rights reserved.
doi:10.1016/j.jmr.2006.12.015

the inter echo time and the number of echoes that can be recorded are insufficient.

q-Space imaging with PFG-SE or -STE is employed to measure the average propagator or displacement spectrum as a function of the displacement encoding time Δ, $P(R,\Delta)$, on a per voxel basis. Every voxel propagator can then be used to calculate a separate quantitative propagator of the flowing and diffusing fluid that is present in a heterogeneous voxel [10,11], thus giving access to sub-voxel information. By analyzing the propagator dependence on labeling time Δ, the method can be extended to study processes such as restricted diffusion, exchange and dispersion [12–15].

Van Dusschoten et al. [3] were the first to combine CPMG (Carr–Purcell–Meiboom–Gill [16]) and PFG into a single PFG-CPMG imaging experiment, designed to simultaneously measure the T_2, the apparent diffusion constant and the amplitude of different fractions within biological tissues, on a voxel-by-voxel basis. In this case, the PFGs were used to generate diffusion weighted multi-echo images, but no attempt was made to measure flow. Correlated flow-T_2 imaging will be harder to do, because one has to preserve the phase information related to coherent displacements in the echo train.

Britton et al. [17] combined q-space displacement encoding and CPMG in a non-imaging PFG-STE-CPMG sequence. In this case, a Fourier transform with respect to the wavevector $q = \gamma\delta g/2\pi$ was used to produce a propagator for every echo in the CPMG train. The two-dimensional experiment thus produced a joint probability density/joint propagator, $P_\Delta(R, t_{\text{echo}})$, that could be transformed into a T_2 resolved propagator $P_\Delta(R, T_2)$ by means of a regularized Laplace inversion for each displacement R. In this example a T_2 resolved propagator was produced by recording long echo trains with a large number of repetitions and a minimum of 16 phase cycles. The large number of phase cycles were needed to preserve the flow related phase information in both the real and imaginary part of the echoes. Without imaging this is no problem. However, when one would aim to perform the same experiment in imaging mode, the number of phase cycles would need to be drastically reduced in order to keep total measurement time within reasonable limits.

Recently, Manz [18] presented a fast multi-echo imaging sequence designed to measure T_2 as well as displacement. In this case the aim of the sequence was to reduce scan time, not to measure correlated displacement and spin–spin relaxation. The sequence was used to measure either T_2 relaxation, by acquiring multiple echoes in a flow insensitive fashion, or to measure flow by using the echo train to acquire multiple q-space displacement encoding steps, but not both at the same time. Doing so, T_2 and flow can only be correlated for the total voxel and no sub-voxel information is obtained.

In this paper, we present a PFG-MSE sequence that can be used to record a true joint propagator on a voxel-by-voxel basis. In order to test the new sequence, we have applied it to a number of flow conducting experimental systems, including a large, intact living plant. Using these examples, we demonstrate that PFG-MSE can be used to record reliable T_2 resolved propagators on a per voxel basis and thus gives access to sub-voxel information with regard to displacement as well as T_2 relaxation behavior in heterogeneous porous media. In addition, PFG-MSE can be used to aid flow quantification in terms of volume flow by making it possible to correct for T_2 relaxation during displacement labeling in PFG displacement imaging methods.

2. Methods

2.1. Pulse sequence

Fig. 1 shows a schematic representation of the Pulsed Field Gradient-Multi Spin Echo (PFG-MSE) sequence. The sequence is based on a modified CPMG sequence that was published earlier by Edzes et al. [19]. PFG displacement encoding was added to the sequence, along the lines set out by Scheenen et al. for their Pulsed Field Gradient-Turbo Spin Echo (PFG-TSE) sequence [10]. For PFG-MSE, the advantage of having the ability to rapidly acquire multiple scan lines per excitation as in PFG-TSE is traded in, at the expense of acquisition time, for the ability to record the T_2 decay for every displacement step in an experiment.

After a slice-selective 90° 3-lobe sinc pulse of 0.5 ms, the magnetization in the XY plane is displacement encoded with two ramped PFGs of length δ in the slice direction, separated by a labeling time Δ. The amplitude g of the PFGs is varied from $-g_{\max}$, via 0, to $+g_{\max}$ in m steps, sampling q-space completely. In between, one or more

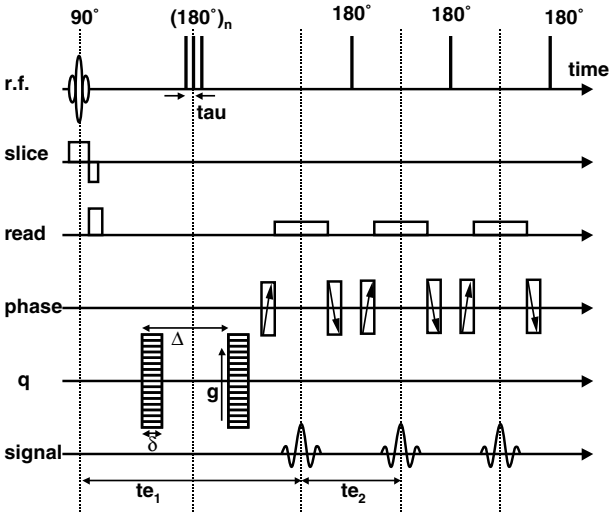

Fig. 1. Schematic representation of the Pulsed Field Gradient-Multi Spin Echo imaging sequence (PFG-MSE). The sequence is based on the modified CPMG sequence published earlier by Edzes et al. [19]. The CPMG sequence was combined with PFG displacement encoding to yield PFG-MSE.

(depending on Δ) additional 180° block pulses of 0.04 ms are inserted, with a variable spacing τ, to overcome susceptibility artifacts [20]. In the modified CPMG spin echo train that follows displacement encoding, every echo is phase encoded and subsequently reverse encoded. In order to maintain the phase information imposed by the two PFGs throughout the echo train a phase cycling scheme is needed. Three phase cycling schemes were employed and compared: CPMG, MLEV-4 $(x\ -x\ -x\ x)_n$ [21], and XY-8 $(x\ y\ x\ y\ -y\ -x\ -y\ -x)_n$ [22]. Hard 180° block pulses are used for two reasons. Firstly, the short duration of the hard pulses allows the use of short echo times, minimizing susceptibility effects [19] and making it possible to acquire many echoes. Secondly, because all spins inside the RF coil experience the non-slice selective pulse, the outflow of spins during the period Δ and during the acquisition of long echo trains is avoided.

2.2. Demonstrators

A phantom, an X-shaped connector, and a 90 cm tall intact tomato plant were used as test objects and demonstrators. The phantom consisted of a central tube with an inner diameter of 6 mm containing flowing water, surrounded by six smaller reference tubes filled with doped water. Three tubes contained a solution with a short T_2 (313 ms), the other three contained a solution with a long T_2 (998 ms). A constant flow of 0.05 ml water per second was maintained in the central tube by means of a Pharmacia Biotech P-500 syringe pump (Amersham Biosciences Europe, Orsay, France). The T_2 of the water pumped through the central tube was varied by using solutions of 2.00, 1.00, 0.50, and 0.25 mM GdDTPA (Schering BV, Weesp, the Netherlands).

The second object, an "X" shaped connector, was used to study the mixing of two fluids of different T_2's (Fig. 2). The connector (code 1412, Kartell, Noviglio (MI), Italy) had an inner diameter of 4.6 mm, 90° angles between the legs, with each leg of the connector having a length of 42 mm. Through leg A a solution of ~6 mM $CuSO_4$ was fed into the connector, through leg B a solution of ~10 mM $CuSO_4$. After crossing the center of the connector, the mixture was allowed to flow out through the opposing two legs.

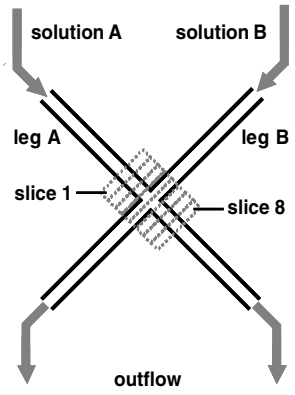

Fig. 2. Mixing of two fluids of different T_2's in an X-shaped connector. Through leg A a solution of 6 mM $CuSO_4$ was fed into the connector, through leg B a solution of 10 mM $CuSO_4$. Two multi-slice PFG-MSE experiments were done, one measuring eight stacked slices along one axis as indicated in the diagram, plus an identical measurement along the other axis (slices not shown).

The third test object, a tomato plant, was grown in a climate chamber (22 °C, 50% RH, 16 h photoperiod 200 μmol m^2 s^{-1} PAR; 20 °C, 50% RH 8 h dark period) on a perlite substrate with a continuous feed of commercially available growth medium. Two weeks before the measurements took place the plant was transferred to water culture. The plant was placed in a 10 l container filled with growth medium and continuously aerated. Before measurements the main stem of the plant was fitted with an RF coil at a height of 15 cm above the pot, and placed upright in the MRI setup. The plant was then left to acclimate in the magnet for two full days. Inside the magnet the plant was subjected to a day period of 14 h at 25 °C and 45% RH at a light intensity of 200 μmol m^2 s^{-1} PAR, and a night period of 10 h at 22 °C and 40% RH.

2.3. MRI spectrometer

In this study, two spectrometers were used. For the phantom and the tomato plant a 0.7 T MRI system based on a Bruker Avance (Bruker, Karlsruhe, Germany) console was used, in combination with a 10 cm air gap Bruker electromagnet (Bruker, Karlsruhe, Germany). For details of this system see [26]. The phantom was inserted into a close fitting custom-built solenoid RF coil. For the tomato plant a solenoid coil was fitted directly around the stem, by placing a thin plastic mould on the stem of the plant and wrapping the coil around the mould.

For the X-shaped connector a 50 cm vertical bore 3 T MRI imager was employed (Bruker, Karlsruhe, Germany). A 14 cm inner diameter gradient insert with up to 0.27 T/m (X, Y, and Z direction) gradient strengths with a rise time of 320 μs was used in combination with a quadrature birdcage RF coil with an inner diameter of 10 cm.

2.4. Signal processing

The joint propagator $P_\Delta(R, t_{\text{echo}})$ datasets that were acquired using the PFG-MSE sequence consisted of a set of conventional complex k-space images, containing a full 2D dataset per voxel with displacement and relaxation information (typically 32 q-space steps by 96 spin echoes). The 2D dataset can be analyzed in different ways. Here, we chose to use the displacement information to separate different pools of water on the basis of displacement, to subsequently analyze relaxation behavior per displacement step. All data handling was performed with home-built software written in IDL (RSI, Boulder, Colorado).

The complex k-space data were Fourier transformed to produce a four-dimensional image matrix containing

q-space images in one dimension and the corresponding echo images in the other. Taking only signal from stationary water in the images into account and handling the even and odd echoes separately, phase corrections with regard to k- as well as q-space were calculated and applied to every echo- and PFG-step in the dataset. After phasing the odd echoes were mirrored in the PFG direction and shifted one gradient step [10]. The whole dataset was then Fourier transformed in the PFG direction in order to yield multi-echo propagator images. All Fourier transforms were done without filtering or zero-filling.

Due to the low field strength of the 0.7 T MRI setup and the small voxel volumes SNR was limited. Especially in cases where only a part of the signal within a voxel originates from flowing water molecules, such as is the case in plants and some porous media, the signal of the flowing water in a voxel is smeared out in the displacement spectrum, further lowering SNR per displacement step. In these cases SNR could be greatly improved by summing multiple voxels in a region of interest (ROI) to yield a two-dimensional dataset containing a one-dimensional propagator for every recorded echo. This way the available spatial resolution is used to construct masks and separate the signal within a ROI from signal originating elsewhere. Flow masks were constructed on the basis of average linear velocity maps, which in turn were constructed from a summation of the first four echoes of the echo-propagator images within the displacement–T_2 dataset. The quantitative velocity maps were calculated using the quantification method as described by Scheenen et al. [10].

Prior to fitting PFG-MSE datasets on a per voxel basis, noise was removed from the multi-echo propagator images by discarding data from voxels that contained a value of zero or lower in the first eight echoes. T_2 decay was fitted using a mono-exponential decay function, yielding quantitative amplitude, $1/T_2$ and T_2. In the analysis, only the real part of the (phase corrected) signal was used. In order to save time in data processing the multi-echo displacement data points were evaluated before mono-exponential fitting. When a decay curve was found to start with a negative value, consisted of less than two positive data points, or was found not to decay, it was assumed to consist of random noise only and was discarded.

3. Results and discussion

3.1. Phantom study

In order to test the ability of the new sequence to measure accurate T_2 values and T_2 independent volume flow rates (the latter by extrapolating the mono-exponential T_2 fits to zero time, providing a quantitative value for proton density over the full range of displacements of a propagator), measurements were done on a phantom consisting of a tube with slowly flowing water, surrounded by six smaller reference tubes filled with stagnant doped water. Amplitude and T_2 maps of this phantom are presented in Fig. 3. A continuous laminar flow of water was maintained in the central tube, the T_2 of which was varied by changing the concentration of GdDTPA from 0.25 to 2.00 mM in four steps.

In order to characterize the flow of water in the phantom, a series of turbo spin echo flow measurements were conducted using the PFG-TSE method [10]. One-dimensional propagators were constructed by summing, respectively, the voxels from the flow conducting tube and the two types of reference tubes (Fig. 4). The propagators of the stagnant solution in the reference tubes exhibited a clean gaussian shape, symmetrical around zero. The propagators of the different solutions that were flowing through the central tube displayed the broadened boxcar profile that is typical for laminar flow through a cylinder, broadened by self-diffusion [11,23]. In a 6 mm tube that conducts a water flow of 0.05 ml/s, Hagen-Poiseuille predicts an average displacement of 0.053 mm at a flow labeling time

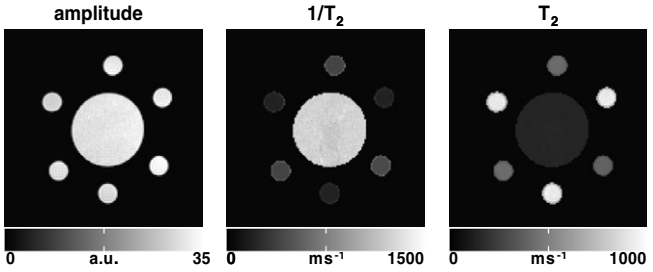

Fig. 3. Amplitude and T_2 maps of the phantom.

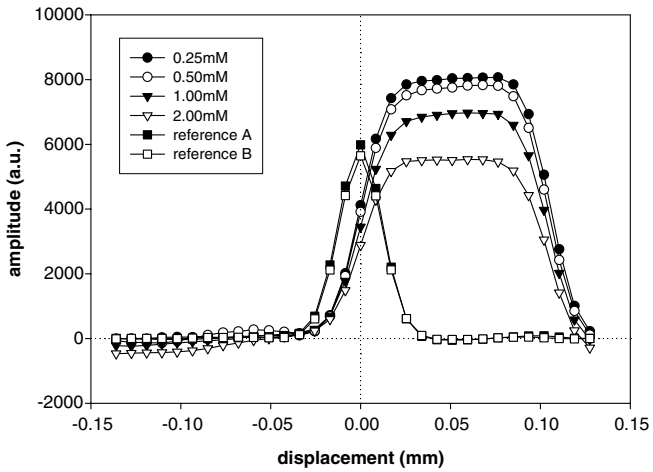

Fig. 4. 1D propagators, constructed from a series of PFG-TSE imaging experiments. The 1D propagators represent the sum total of all signal originating from the two sets of reference tubes, shown in Fig. 3 (square markers) or the central flow conducting tube (round and triangular markers). Amplitude and T_2 maps of this object are shown in Fig. 3. Four solutions with an increasing concentration of GdDTPA were pumped through the central tube, 0.25 mM (closed circles), 0.5 mM (open circles), 1 mM (closed triangles) and 2 mM (open triangles). Experimental parameters: 64×64 matrix, field of view 16.5 mm, slice thickness 3 mm, two averages, repetition time 5 s, TE 4.95 ms; 32 PFG steps, labeling time Δ 30 ms, PFG duration δ 3 ms, PFG_{max} 0.461 T m^{-1}, during Δ 3 180° pulses, τ 5.25 ms; measurement time 43 min.

of 30 ms, corresponding closely to the average displacements that were measured. For the 0.25, 0.5, 1.0, and 2.0 mM GdDTPA solutions average displacements of 0.052, 0.051, 0.051, and 0.050 mm was measured, respectively.

In our PFG-TSE sequence, k-space was sampled from the center ($k = 0$) outward. Doing so, the effective echo time, and thus propagator amplitude, is determined by the first echo after the displacement labeling period [10]. During flow labeling in a PFG-SE or PFG-TSE experiment the magnetization is subjected to T_2 decay. The effect of T_2 relaxation during flow labeling became more noticeable with increasing solute concentration. The amplitude difference between the propagators of the reference tubes and the 0.25 and 0.5 mM solutions remained small, but T_2 relaxation effects became especially noticeable in the propagators of the 1.0 and 2.0 mM solutions. When the T_2 of the flowing fluid is not known, for instance in the case of fluid flow through a micro-porous material, T_2 relaxation effects like these would exclude a proper quantification of volume flow.

Since we wished to analyze relaxation behavior, the stability of the echo-propagators throughout the echo train was of paramount importance. It is well known from literature that displacement encoding interferes with the CPMG conditions, resulting in a rapid loss of transverse coherence [22,24,25]. Maintaining both components (real and imaginary) of transverse magnetization is essential for flow imaging, because it is needed to determine the direction of flow. Phase cycling schemes other than the classical CPMG have been shown to be effective in avoiding this loss of coherence. Here, three phase cycling schemes were tested, CPMG, MLEV-4 $(x\ -x\ -x\ x)_n$ [21], and XY-8 $(x\ y\ x\ y\ -y\ -x\ -y\ -x)_n$ [22].

When a CPMG phase cycling scheme was employed, the echo-propagators lost phase coherence after as few as four echoes (Fig. 5a). At this point in the echo train the displacement images of the flowing water started to appear not only on the right-hand side, but also on the left-hand side. This indicates that the phase coherence of the transverse signal was lost, because of which the direction of flow could no longer be determined. The application of an MLEV-4 phase cycling scheme brought about a slight improvement, but it also resulted in a wave pattern in which the displacement images of the flowing water first (correctly) appeared on the right-hand side, but then, as the echo train progresses, the displacement images shifted from the right to the left, and back again (Fig. 5b). In contrast to the two previous phase cycling schemes, XY-8 was very effective in preserving the displacement information throughout the length of an echo train (Fig. 5c). The echo-propagators remained stable from echo 1 to echo 128. Gullion et al. found that during XY-8 the longitudinal and transverse components of the magnetization are treated identically, compensating the loss of phase coherence in both. During MLEV phase cycling this is not the case. MLEV was found to behave well in shorter echo trains, but in longer echo trains failed to compensate both components of the magnetization [22]. This corresponds well with our observations. We therefore used the XY-8 phase scheme in all subsequent experiments.

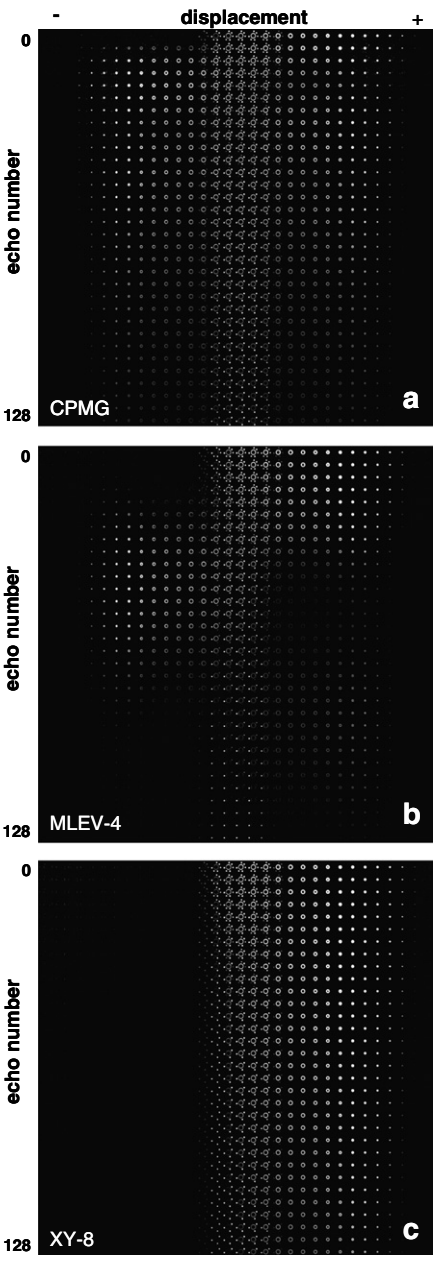

Fig. 5. A comparison of multi-echo propagator images acquired with the PFG-MSE sequence, using the CPMG (a), MLEV-4 (b) and XY-8 (c) phase cycling schemes. The displacement direction runs from left to right with zero displacement in the center, while echo images are displayed from top to bottom. For compactness, the 128 echoes that were acquired were reduced to 32 in this figure, by averaging sets of four echoes. Experimental parameters: 32×32 matrix, field of view 16.5 mm, slice thickness 3 mm, two averages, repetition time 2.5 s; 32 PFG steps, labeling time Δ 30 ms, PFG duration δ 3 ms, PFG_{max} 0.46 T m^{-1}.

To test the ability to measure accurate T_2 values, solutions of different T_2's were pumped through the central tube of the phantom object. Fig. 6 shows the results of mono-exponential fits, done on the sum total of all signal

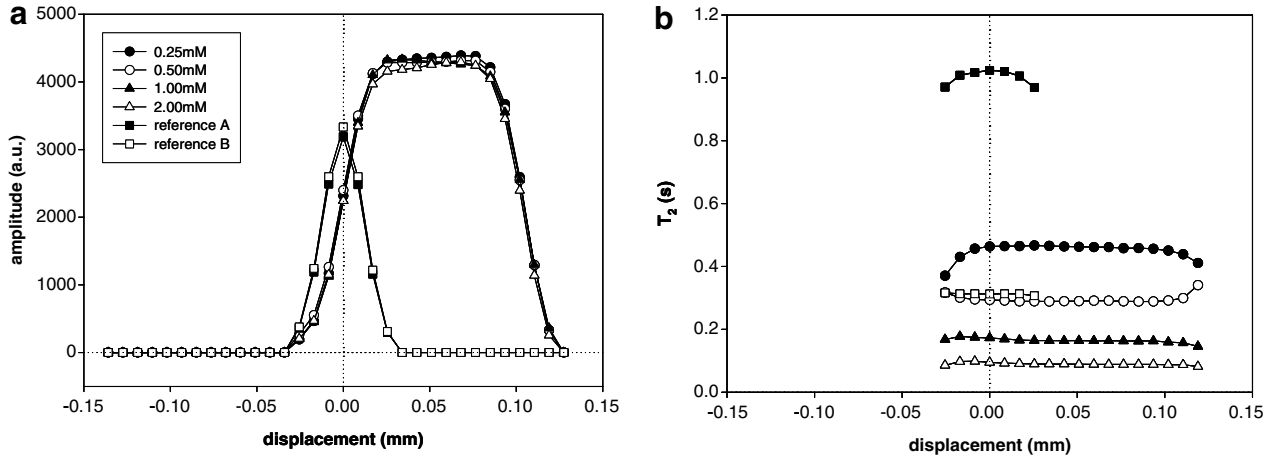

Fig. 6. The results of mono-exponential fits of the sum total of all signal originating from the two sets of reference tubes and on the four different solutions flowing in the central tube of the phantom, 0.25, 0.5, 1, and 2 mM GdDTPA. (a) The amplitudes $A(R)$; in (b) the values obtained for $T_2(R)$ are shown. The amplitude (A) and T_2 values were obtained by fitting the decays for each displacement step $R(\Delta)$ using a mono-exponential fit as described in the text. Experimental parameters: 64×64 matrix, field of view 16.5 mm, slice thickness 3 mm, two averages, repetition time 5 s, 96 echoes, TE 4.95 ms; 32 PFG steps, labeling time Δ 30 ms, PFG duration δ 3 ms, PFG_{max} 0.46 T m^{-1}, during Δ 5 180° pulses, τ 5.25 ms; measurement time 5.45 h.

within different ROI's of the phantom. The T_2 values of the reference tubes and the flowing solutions remained virtually constant over the full widths of their respective propagators, only showing appreciable variation at the far ends of the propagators, where signal intensity became too low to give reliable results (Fig. 6b). The T_2 values of the water in the two sets of reference tubes corresponded well with the values measured in a flow-insensitive T_2 imaging experiment (compare Fig. 6b with Fig. 4), and with the T_2 values found using (non-imaging) relaxometry (data not shown), indicating that the measured T_2 values were accurate.

The results of the PFG-TSE measurements presented in Fig. 4 provide a good indication of the amount of signal that can be lost due to spin–spin relaxation during flow encoding when the T_2 of the flowing solution is lowered, even during a flow labeling period as short as 30 ms. One of the major advantages of PFG-MSE is that it makes it possible to calculate the amplitude at $t = 0$ for every single displacement step, thus eliminating the effects of signal decay during the labeling time, as was demonstrated in Fig. 6a. The extrapolated amplitudes of the different flowing solutions match closely, regardless of the T_2 of the solutions involved.

In Fig. 7, it is demonstrated that it is possible to analyze the PFG-MSE data on a per voxel basis. The measurement was done on the same object as before, but in this example a solution of 2 mM GdDTPA was pumped through the phantom. A mono-exponential fit of the echo train associated with every voxel of every displacement step yielded quantitative amplitude–displacement (A–R) maps (Fig. 7a), $1/T_2$–displacement ($1/T_2$–R) maps (Fig. 7b) and T_2–displacement (T_2–R) maps (Fig. 7c). Displacements ranging from −0.136 to 0.127 mm were recorded, but in order to save space only signal containing displacement images (ranging from −0.026 to 0.127 mm) are shown. Extrapolation of the mono-exponential T_2 fits to $t = 0$ yielded clean proton density (amplitude, A) maps (Fig. 7a), with the signal from the stagnant water in the reference tubes centered around zero displacement, and the characteristic pattern of rings of the laminar upward flowing water in the central tube to the right-hand side of zero displacement. The T_2 of the flowing water in this example was short compared to the T_2's of the stagnant water in the reference tubes. Therefore, the flowing water was clearly visible in the displacement-$1/T_2$ maps (Fig. 7b), but not in the displacement–T_2 maps (Fig. 7c). The T_2 as well as

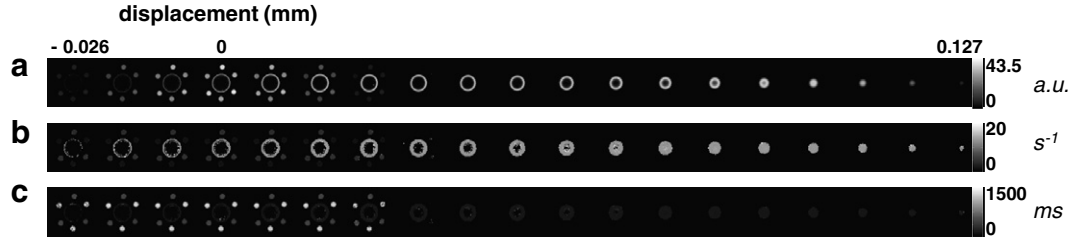

Fig. 7. Amplitude–displacement (A–R; (a)), $1/T_2$–displacement ($1/T_2$–R; (b)) and T_2–displacement maps (T_2–R; (c)) of the phantom conducting a solution of 2 mM GdDTPA. The amplitude and T_2 values were obtained by fitting the decays for each voxel and each displacement step $R(\Delta)$, using a mono-exponential fit as described in the text. For experimental parameters see Fig. 6. Thirteen displacement images on the left, from −0.136 to −0.034 mm, do not contain useful information and are not shown.

$1/T_2$ values of the flowing and stationary fluids were consistent throughout the displacement range.

3.2. Mixing fluids in an X-shaped connector

The possibility to use the PFG-MSE sequence to study the mixing of fluids was tested on an experimental setup in which an X-shaped conduit was used to bring two solutions of different T_2 into contact (Fig. 2). As shown in the figure, two times eight stacked slices were measured, first along the axis of one of the legs, then along the axis of the other. Through leg A a solution of (approx.) 6 mM $CuSO_4$ was flowing into the connector, through leg B a solution of (approx.) 10 mM $CuSO_4$. At the junction the two fluids are forced to mix or cross each other. In this experiment, we aimed to image the two fluids as they were mixing inside the X-shaped connector, and determine whether or not turbulent mixing took place.

The inflow velocities of both solutions were of comparable magnitude, although the 10 mM solution (Fig. 8, leg A, slice 1) was flowing slightly faster than the 6 mM solution (Fig. 8, leg B, slice 1). At inflow both solutions show a laminar flow profile. The average $1/T_2$ of the 6 mM solution was $4\ s^{-1}$, and $6\ s^{-1}$ for the 10 mM solution. At slice 4, in the center of the connector, a small vortex could be observed (Fig. 8, leg B, slice 4; see arrow). The majority of flow at the crossing point appeared to stay laminar however, with the 6 mM solution (low $1/T_2$) flowing over and on top of the 10 mM solution—instead of next to each other, as might have been expected because of the symmetry of the X-connector. This up–down stratification persisted all the way into the outflow tubes, as can be concluded from Fig. 8b. At slice 8, which was located between 7.5 and 10 mm from the center of the connector, the 6 mM solution was still flowing on top of the 10 mM solution in both outflow tubes, with the $1/T_2$ maps showing a sharp and straight transition between the two solutions.

3.3. Water transport in the stem of tomato

PFG-MSE is especially useful in systems where the spatial resolution is not high enough to resolve individual pores. It offers the possibility to distinguish pools of water within the same voxel on the basis of its displacement behavior, thus giving access to a form of sub-voxel information. An interesting example of such a flow conducting system is the plant stem.

Long distance water transport in plants takes place in two transport systems, the phloem and the xylem. The phloem conducts a small flux of water with photosynthesis products from source (leaves) to sink (roots, fruits, places of growth or maintenance), while the xylem conducts a larger flux of water from the roots to the leaves. The two pathways have in common that transport takes place in vessels that are, in most plants, too small to be resolved with NMR microscopy. As a consequence, a flow conducting voxel may contain one or more vessels or parts of vessels, as well as a significant amount of stationary water,

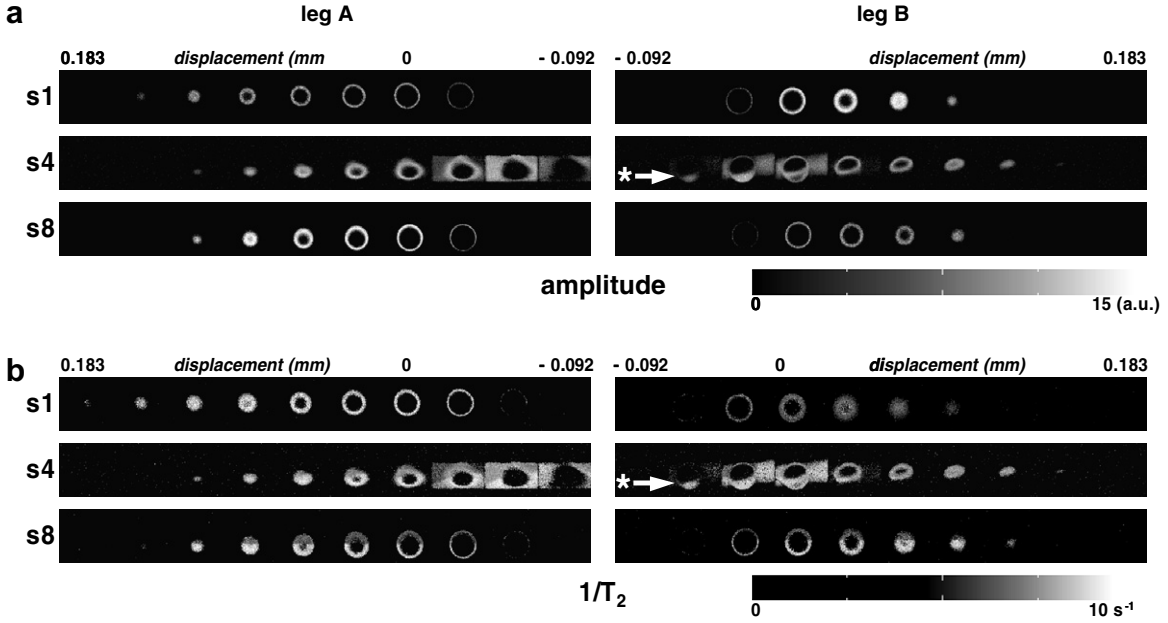

Fig. 8. A–R (a) and $1/T_2$–R maps (b) of six slices on different positions along the two axes of an X-shaped connector (see Fig. 2), acquired using two multi-slice PFG-MSE experiments. Two solutions of different T_2 were fed into the connector on one side, and forced to mix at the junction. Shown are the two slices located at the site of inflow (s1), two slices at the junction (s4), and two slices at the point of efflux. A small vortex in one of the two legs of the connector, at the point where the two fluids mix, is indicated with an asterisk. Experimental parameters: 64×64 matrix, eight slices, field of view 96 mm, slice thickness 2.5 mm, two averages, repetition time 2 s, 20 echoes, TE_2 11 ms; 32 PFG steps, labeling time Δ 40 ms, PFG duration δ 4 ms, PFG_{max} $0.20\ T\ m^{-1}$, during Δ no additional 180° pulses were used; measurement time 2.16 h. To save space only displacement maps that contain useful information are shown.

located in the tissue surrounding the vessel. Using PFG-TSE, we have previously been able to quantitatively measure detailed flow profiles of xylem as well as phloem transport in plants, on a per voxel basis [10,11,26]. In these measurements the stationary water within flow containing voxels was separated from flowing water by making use of the fact that displacement probability distribution of stationary water is symmetrical around zero, whereas the propagator of flowing water is not. If the direction of flow is positive, subtracting the negative half of the propagator from the positive half will yield the propagator of the flowing water only, or vice versa for negative flow directions. Here, we explored the possibility to do the same for every echo-propagator in a PFG-MSE experiment, in order to separately measure the T_2 relaxation behavior of flowing and stationary water [9].

A summation of the first four echo-propagators was used to identify all flow conducting voxels and construct a flow mask (Fig. 9a, inset). By analyzing all signal present within the flow mask as described earlier, a one-dimensional calculated propagator and a corresponding T_2–R plot was obtained (Fig. 9a). The shape of the resulting propagator was typical for water transport in plant tissue. Centered around zero displacement, a large amount of stationary water was observed, while the flowing xylem water was visible to the right-hand side of the propagator with displacements of up to 0.112 mm. Large differences in T_2 were observed, ranging from 0.13 s around 0 displacement, to 0.37 s at 0.122 mm displacement; an almost threefold increase. Between a displacement of 0 and 0.031 mm, T_2 will have been influenced by the contribution of the pool of (diffusing) stationary as well as the pool of flowing water, because in this range of displacements both pools of water are present. In order to allow the relaxation behavior of both pools to be evaluated independently, the stationary water was separated from the flowing water for every echo-propagator in the dataset, following the method described by Scheenen et al. [10,11]. Analyzing the resulting two multi-echo-propagator datasets as before yielded the A–R and T_2–R plots shown in Fig. 9b. The T_2 of stationary water in tissue surrounding the flow conducting vessels was clearly shorter than the T_2 of the flowing water, even at low displacements. The T_2 of the flowing water molecules increased markedly with increasing displacement, water with the largest displacements having the highest T_2 value.

In tomato, xylem water is transported through a few large vessels and many smaller ones. It is generally assumed that xylem flow is laminar, although xylem vessels can exhibit large differences in diameter, resulting in an unpredictable flow profile when multiple vessels are present within a voxel or an ensemble of voxels. The pressure difference that is driving xylem flow can be assumed to be approximately equal for all xylem vessels, because a great number of axial connections are present between vessels and bundles of vessels along the length of the stem. In this system, the fastest flowing water would be found in the center of the largest vessels, whereas slower flowing water would be expected in the smaller vessels and in the vicinity of the vessel wall of larger vessels. Because the intrinsic T_2 of xylem water is long (up to 1 s) and T_2 is expected to decrease with decreasing vessel diameter [7,17,27–30], it is likely that the relationship between displacement and T_2 reflects the vessel size distribution in the plant stem—although vessel wall permeability and exchange processes may also influence the T_2–displacement profile.

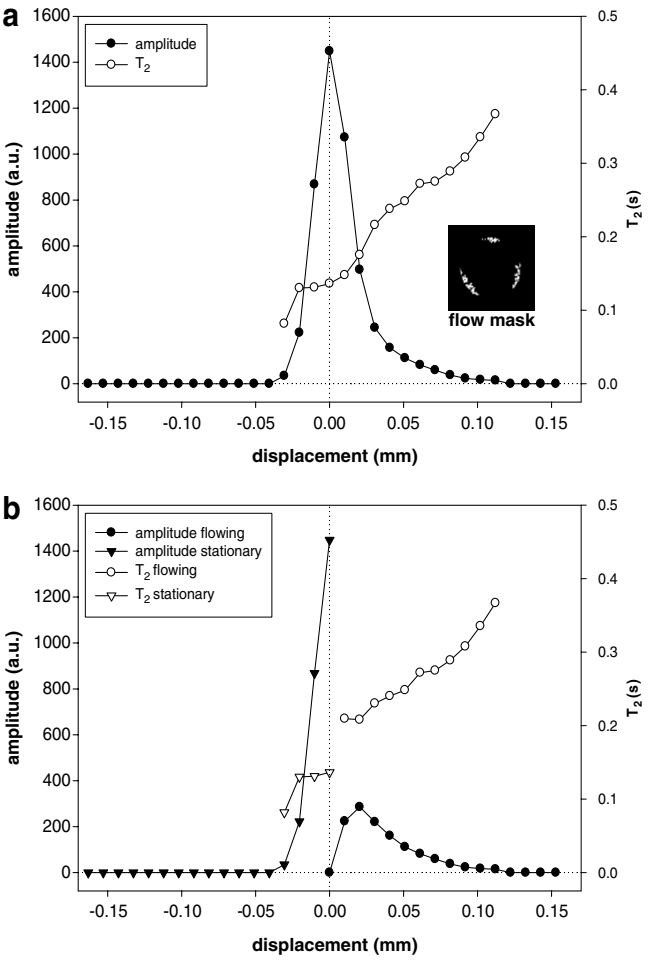

Fig. 9. The amplitudes, $A(R)$ and T_2 values, $T_2(R)$ for all flowing xylem water within the flow mask (see inset). In (a) the amplitude (closed symbols) and T_2 (open symbols) values are shown for all signal within the flow mask. In (b) the same is shown, but previous to mono-exponential fitting stationary and flowing water were separated by making use of the fact that water that is not flowing is symmetrical around zero displacement, as described in the text. Experimental parameters: 128×64 matrix, field of view 15 mm, slice thickness 3 mm, two averages, repetition time 2.5 s, 64 echoes, TE_2 5.81 ms; 32 PFG steps, labeling time Δ 30 ms, PFG duration δ 3 ms, PFG_{max} 0.46 T m^{-1}, during Δ three 180° pulses, τ 9.1 ms; measurement time 2.50 h.

The next step was to separate stationary and flowing water protons on a per voxel basis. Mono-exponential fitting yielded A–R maps, $1/T_2$–R maps, and T_2–R maps of stationary (Fig. 10) and flowing water (Fig. 11). To reduce the size of the figures only displacement maps that contain signal are shown. In the $1/T_2$ and T_2 images the difference

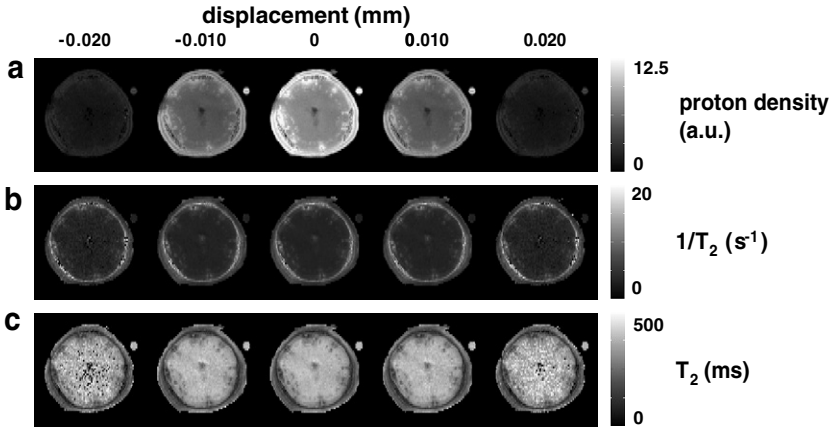

Fig. 10. A–R (a), $1/T_2$–R (b) and T_2–R maps of a transverse slice of the stem of an intact tomato plant, showing only stationary water. Previous to voxel-by-voxel fitting, the acquired joint propagator $P_\Delta(R, t_{\text{echo}})$ was used to construct two datasets containing either stationary or flowing water. To save space only displacement maps that contain useful information are shown. For experimental parameters see Fig. 9.

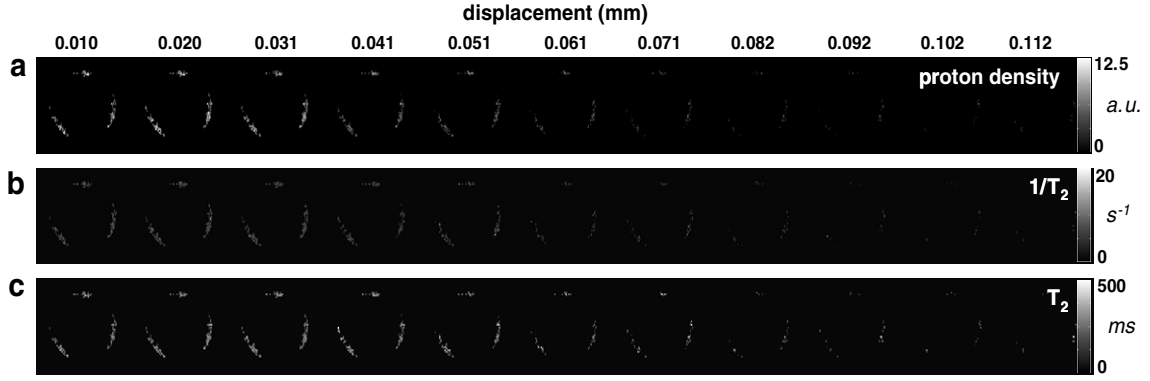

Fig. 11. A–R (a), $1/T_2$ (b) and $1/T_2$ (c) maps of a transverse slice of the stem of an intact tomato plant, showing only flowing water. To save space only displacement maps that contain useful information are shown. Experimental parameters: see Fig. 9.

between the T_2 of the flowing and stationary water can be seen as well. In Fig. 10c the xylem tissue became visible as dark regions with low T_2 values, whereas in Fig. 11c the flowing water is much brighter. In the absence of other structures for reference, the relationship between T_2 and displacement that was clearly visible in Fig. 9b was harder to see in imaging mode. The A–R maps of the stationary water in the plant in Fig. 10 could be used to calculate maps of proton density and diffusion constant, as is demonstrated in Fig. 12. In this example a gauss was fitted to the displacement spectrum of the stationary fraction (Fig. 10a). The apparent diffusion constant was then calculated from the width of the gauss.

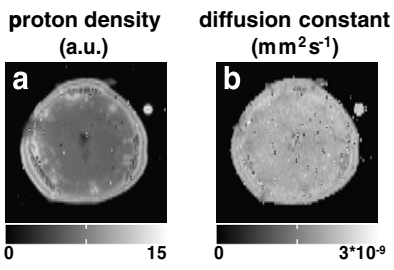

Fig. 12. Maps of amplitude (a) and diffusion constant (b), calculated from the stationary amplitude–displacement maps shown in Fig. 10.

4. Conclusion

In this paper, a PFG-MSE sequence with an XY-8 phase scheme in the echo train has been presented, that can be used to perform spatially resolved correlated displacement T_2 imaging, by recording a correlated voxel propagator $P_\Delta(R, t_{\text{echo}})$ on a per voxel basis. It has been shown that these T_2 resolved propagators make it possible to calculate quantitative A–R, $1/T_2$–R and T_2–R maps.

PFG-MSE makes it possible to first separate protons that reside within the same voxel on the basis of displacement, and subsequently measure their T_2 relaxation behavior. This gives access to a wealth of information on a sub-voxel level, making PFG-MSE especially useful in spatially heterogeneous porous systems, where the spatial resolution that can be obtained is not high enough to resolve the structure. The coupled flow and relaxation information can be used to simply correct for relaxation

during displacement labeling in PFG displacement imaging experiments, when the objective of an experiment is to quantify volume flow, but it also provides a tool to study correlations between displacement and T_2 relaxation. The latter offers interesting opportunities, as spin–spin relaxation can yield information on a range of parameters that are of interest when dealing with flow and diffusion related subjects, such as vessel or pore size distribution and geometry, exchange processes, permeability changes, emulsions, or fluid mixing. A drawback of the method is the long measurement time that it requires, depending on the experimental parameters that are chosen.

Acknowledgments

We wish to thank prof. T.J. Schaafsma and prof. H. van Amerongen for critically reading this manuscript. This research was supported by the Dutch Technology Foundation STW, the applied science division of NWO, Project No. WBI 4803.

References

[1] J.B. Aguayo, S.J. Blackband, J. Schoeniger, M.A. Mattingly, M. Hintermann, Nuclear magnetic resonance imaging of a single cell, Nature 322 (1986) 190–191.
[2] S.C. Lee, K. Kim, J. Kim, S. Lee, J.H. Yi, S.W. Kim, K.S. Ha, C. Cheong, One micrometer resolution NMR microscopy, J. Magn. Reson. 150 (2001) 207–213.
[3] D. van Dusschoten, C.T. Moonen, P.A. de Jager, H. Van As, Unraveling diffusion constants in biological tissue by combining Carr–Purcell–Meiboom–Gill imaging and pulsed field gradient NMR, Magn. Reson. Med. 36 (1996) 907–913.
[4] P.N. Sen, Time-dependent diffusion coefficient as a probe of geometry, Concepts Magn. Reson. A 23A (2004) 1–21.
[5] Y. Qiao, P. Galvosas, P.T. Callaghan, Diffusion correlation NMR spectroscopic study of anisotropic diffusion of water in plant tissues, Biophys. J. 89 (2005) 2899–2905.
[6] M.D. Does, J.C. Gore, Compartmental study of diffusion and relaxation measured in vivo in normal and ischemic rat brain and trigeminal nerve, Magn. Reson. Med. 43 (2000) 837–844.
[7] M.M. Britton, R.G. Graham, K.J. Packer, NMR relaxation and pulsed field gradient study of alginate bead porous media, J. Magn. Reson. 169 (2004) 203–214.
[8] P.T. Callaghan, Principles of Nuclear Magnetic Resonance Microscopy, Oxford University Press, New York, 1993.
[9] F.R.E. Fenrich, C. Beaulieu, P.S. Allen, Relaxation times and microstructures, NMR Biomed. 14 (2001) 135–139.
[10] T.W.J. Scheenen, D. van Dusschoten, P.A. de Jager, H. Van As, Microscopic displacement imaging with pulsed field gradient turbo spin-echo NMR, J. Magn. Reson. 142 (2000) 207–215.
[11] T.W.J. Scheenen, D. van Dusschoten, P.A. de Jager, H. Van As, Quantification of water transport in plants with NMR imaging, J. Exp. Bot. 51 (2000) 1751–1759.
[12] J. Pfeuffer, U. Flogel, D. Leibfritz, Monitoring of cell volume and water exchange time in perfused cells by diffusion-weighted H-1 NMR spectroscopy, NMR Biomed. 11 (1998) 11–18.
[13] Y. Cohen, Y. Assaf, High *b*-value q-space analyzed diffusion-weighted MRS and MRI in neuronal tissues - a technical review, NMR Biomed. 15 (2002) 516–542.
[14] U. Tallarek, F.J. Vergeldt, H. Van As, Stagnant mobile phase mass transfer in chromatographic media: Intraparticle diffusion and exchange kinetics, J. Phys. Chem. B 103 (1999) 7654–7664.
[15] U. Tallarek, E. Rapp, A. Seidel Morgenstern, H. Van As, Electro-osmotic flow phenomena in packed capillaries: from the interstitial velocities to intraparticle and boundary layer mass transfer, J. Phys. Chem. B 106 (2002) 12709–12721.
[16] H.Y. Carr, E.M. Purcell, Effects of diffusion on free precession in nuclear magnetic resonance experiments, Phys. Rev. 94 (1954) 630–638.
[17] M.M. Britton, R.G. Graham, K.J. Packer, Relationships between flow and NMR relaxation of fluids in porous solids, Magn. Reson. Imaging 19 (2001) 325–331.
[18] B. Manz, Combined relaxation and displacement experiment: a fast method to acquire T_2, diffusion and velocity maps, J. Magn. Reson. 169 (2004) 60–67.
[19] H.T. Edzes, D. van Dusschoten, H. Van As, Quantitative T2 imaging of plant tissues by means of multi-echo MRI microscopy, Magn. Reson. Imaging 16 (1998) 185–196.
[20] D. van Dusschoten, P.A. de Jager, H. Van As, Flexible PFG NMR desensitized for susceptibility artifacts using the PFG-multiple-spin-echo sequence, J. Magn. Reson. A (1995) 237–240.
[21] A.J. Shaka, S.P. Rucker, A. Pines, Iterative Carr–Purcell trains, J. Magn. Reson. 77 (1988) 606–611.
[22] T. Gullion, D.B. Baker, M.S. Conradi, New, compensated Carr–Purcell sequences, J. Magn. Reson. 89 (1990) 479–484.
[23] U. Tallarek, E. Rapp, T. Scheenen, E. Bayer, H. Van As, Electro-osmotic and pressure-driven flow in open and packed capillaries: velocity distributions and fluid dispersion, Anal. Chem. 72 (2000) 2292–2301.
[24] P. Le Roux, Non-CPMG fast spin echo with full signal, J. Magn. Reson. 155 (2002) 278–292.
[25] M.E. Bastin, P. Le Roux, On the application of a non-CPMG single-shot fast spin-echo sequence to diffusion tensor MRI of the human brain, Magn. Reson. Med. 48 (2002) 6–14.
[26] C.W. Windt, F.J. Vergeldt, P.A. De Jager, H. Van As, MRI of long-distance water transport: a comparison of the phloem and xylem flow characteristics and dynamics in poplar, castor bean, tomato and tobacco, Plant Cell Environ. 29 (2006) 1715–1729.
[27] L. van der Weerd, M.M.A.E. Claessens, T. Ruttink, F.J. Vergeldt, T.J. Schaafsma, H. Van As, Quantitative NMR microscopy of osmotic stress responses in maize and pearl millet, J. Exp. Bot. 52 (2001) 2333–2343.
[28] L. van der Weerd, S.M. Melnikov, F.J. Vergeldt, E.G. Novikov, H. Van As, Modelling of self-diffusion and relaxation time NMR in multicompartment systems with cylindrical geometry, J. Magn. Reson. 156 (2002) 213–221.
[29] J.E.A. Reinders, H. Van As, T.J. Schaafsma, P.A. De Jager, D.W. Sheriff, Water balance in Cucumis plants measured by NMR I, J. Exp. Bot. 39 (1988) 1199–1210.
[30] H. Van As, T.J. Schaafsma, Noninvasive measurement of plant water flow by nuclear magnetic resonance, Biophys. J. 45 (1984) 469–472.